

# Cluster dynamics in macroscopic photoactive particles

Sára Lévay,<sup>1,\*</sup> Axel Katona,<sup>1</sup> Hartmut Löwen,<sup>2</sup> Raúl Cruz Hidalgo,<sup>1</sup> and Iker Zuriguel<sup>1</sup>

<sup>1</sup>*Departamento de Física y Matemática Aplicada, Facultad de Ciencias, Universidad de Navarra, E-31080 Pamplona, Spain*

<sup>2</sup>*Institut für Theoretische Physik II: Weiche Materie, Heinrich-Heine-Universität Düsseldorf, D-40225 Düsseldorf, Germany*

(Dated: December 20, 2024)

We present an experimental study on the collective behavior of macroscopic self-propelled particles that are externally excited by light. This property allows testing the system response to the excitation intensity in a very versatile manner. We discover that for low excitation intensities, clustering at the boundaries is always present, even when this is prevented by implementing flower-shaped confining walls. For high excitation intensities, however, clusters are dissolved more or less easily depending on their size. Then, a thorough analysis of the cluster dynamics allows us to depict a phase diagram depending on the number of agents in the arena and the excitation intensity. To explain this, we introduce a simple kinetic model where cluster evolution is governed by a balance between adsorption and desorption processes. Interestingly, this simple model is able to reproduce the phase space observed experimentally.

*Introduction.*— Active matter refers to systems made up of many interacting self-propelled agents that convert energy into mechanical motion, exemplifying out-of-equilibrium systems. This field has gained significant attention over the past few decades due to its broad applications in physics, chemistry, biology, medicine, and robotics. In its broader conception, examples of active matter systems include microrobots [1–5], colloidal particles [6–10], bacterial systems [11, 12], vibrated granular [13–17], robotic swarms [18], animal groups [19, 20], and pedestrians. Despite the variety of constituents and interactions within these systems, they share common properties at the group level. Accordingly, several models have been developed to describe the emergence of collective behavior illustrating the Aristotelian concept that the whole is greater than the sum of the parts.

The energy that drives the motion of active particles can originate directly from the particles themselves, such as in bird flocks, or through an external source as it occurs for microswimmers. Often, this motion is a response to a stimulus, a phenomenon known as taxis. Based on the nature of the driving force, we can differentiate between various types of taxis: chemotaxis [21], thigmotaxis [22], viscotaxis [23], and magnetotaxis [2–4, 24]. When the stimulus is created with light, we have phototactic or photoactive behavior [1, 5, 8–11]. Importantly, all of these systems involve particles whose size lies in the range of microns.

Here we focus in a new scenario in which the active particles responding to an external stimulus (light) are macroscopic (in the scale of centimeters) [25]. This photoactive granular matter is especially interesting as the interactions occur solely through physical contact, facilitating the control and reproduction of experimental conditions. In contrast, this can be challenging in systems

that involve hydrodynamic or social interactions among agents. Moreover, by using a programmable illumination panel, we have complete control over the activity of the agents, enabling us to adjust their behavior in both space and time. While this idea of external control of the activity of the agents is commonly applied to microscopic particles [10, 11], it is pioneering in the context of macroscopic ones. To our knowledge, this approach has only been applied in phototactic wheeled robots [26–28] where the dynamics are clearly different.

Our agents are an evolved version of the HEXBUG

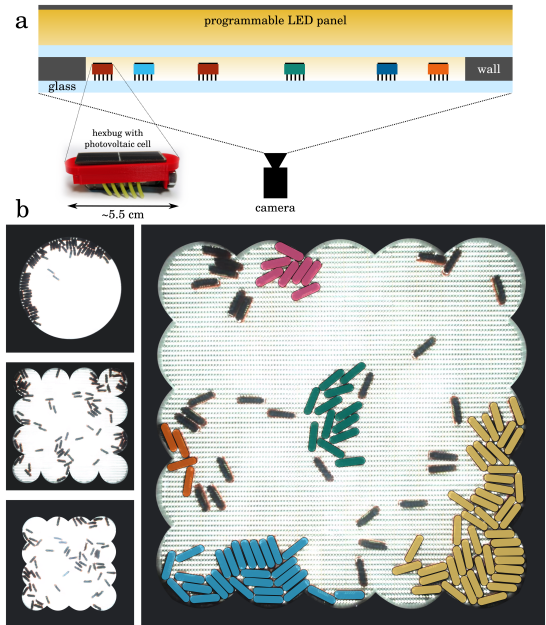


FIG. 1. (a): Scheme of the experimental setup and picture of the photoactive bug. (b): Snapshots of experiments with different walls. The largest snapshot corresponds to the arena used in the main manuscript where different colors are used to identify clusters (see SM Video 1).

\* slevay@unav.es

nano<sup>®</sup> [29], particles that are characterized by displaying a rather persistent directed motion and which have been utilized in studies related to clogging, sorting, traffic jams, robotic superstructures, and resetting [30–39]. An interesting aspect of active particles with persistent directed motion is their tendency to accumulate at the walls [40], hence leading to clustering. Clusters exhibit rich physics, depending on factors like particle shape, driving mechanism, the strength of external forcing, and the interaction between agents. These factors determine the properties of the clusters, such as the size distribution, stability, and internal structure [6, 13, 41–44]. Understanding the mechanisms beyond clustering in active systems is essential not only for theoretical advancements, but also for applications such as programmable materials, biomedical applications, robotic swarms, and environmental sensing. In this paper, we focus on the clustering behavior of photoactive particles under homogeneous illumination investigating the effect of particle activity and particle density.

*Experimental setup and methods.*— Our photosensitive, self-propelled particles have 10 asymmetric soft rubber legs and a vibrating motor, which give rise to a directed movement with velocities depending on the vibration frequency. Originally, the motor was powered by a battery but this was replaced by a 3D-printed plastic cap holding a photovoltaic cell (see Fig. S1 (a)). In this way, the particles (5.5 cm long and 1.5 cm wide) can only move when illuminated. By adjusting the illumination intensity, we can change the vibration frequency and thus control the velocity of the particles in the range of roughly 8 to 14 cm/s.

Our experimental setup is presented in Fig. S1 and in the Supplemental Material (SM) [45]. The agents move on a horizontal glass sheet measuring  $80 \times 80 \text{ cm}^2$  and are enclosed by 3D-printed flower-shaped plastic walls. Various wall structures were tested, as depicted in Fig. S1 (b) and which effect is discussed in the SM. The results described in this paper were obtained using the wall structure in the right panel; which was specifically designed to guide the particles inward and away from the boundaries [46]. Above the arena, another glass sheet is placed at a height such that there is no contact with the bugs during their free motion but prevents tumbling in strong collisions. In some instances, particularly in scenarios with high density and activity, a few particles (less than 5% of the total population) were observed to tumble, hence stopping their motion. The illumination panel ( $80 \times 80 \text{ cm}^2$ ) is made of LED lines mounted on an aluminum plate. The lines are controlled by ESP32 microcontrollers, making the panel fully programmable and allowing for the application of illumination fields with temporal and spatial gradients. The imaging system (an Imaging Source DFK-37BUX250 camera) is positioned beneath the setup to record videos at 30 fps in order to track the motion of the particles. Before studying the collective behavior of the agents, we characterized them individually to have detailed information about the il-

lumination intensity dependence of their motion. For details, we refer the reader to the SM.

We used five different population sizes ( $N_T=40, 60, 80, 100$  and  $120$ , the total number of particles in the arena) and seven different illumination intensity levels. The later is quantified by the power ( $P$ ) an individual bug receives through the solar cell; then, the higher the power, the higher the bug activity. For each population size and activity level, we conducted five independent 6-minute-long experiments. Before each experiment, the particles were evenly distributed in rows between the two halves of the arena, facing to the center (see the beginning of SM videos). Then, the light is switched on and the particles start moving. Rapidly, driven by collisions and wall interactions, small clusters start forming either at the central part of the arena or at the boundaries (green, orange, and pink in Fig. S1 (b)). Most of them just dissolved after a few seconds, but others (especially those in the walls) grew and became more stable (blue and yellow in Fig. S1 (b)). In what follows, we present an analysis of the dynamics of these clusters which, in our work, are defined as groups of at least 4 particles that remain in contact for at least 1 second. See the SM for a detailed description of the cluster detection method.

*Results.*— Our observations indicate that clusters become larger and exhibit greater stability when the particle activity is lower and the population size is larger. An evidence of this is presented in Fig. 2, where the time evolution of clusters is reported for three illumination intensities ( $P$ ) and two population sizes ( $N_T$ ). For clarity, only clusters that reach a size ( $N$ ) of at least a third of the total population ( $n=N/N_T \geq 0.33$ ) are colored (different colors are used for each experimental realization). It is evident that higher intensities and lower particle numbers (top-left panel) result in the formation and destruction of small clusters (see SM Video 3 [45]). As particle activity decreases and population size increases, larger, more stable clusters tend to form. Some of these

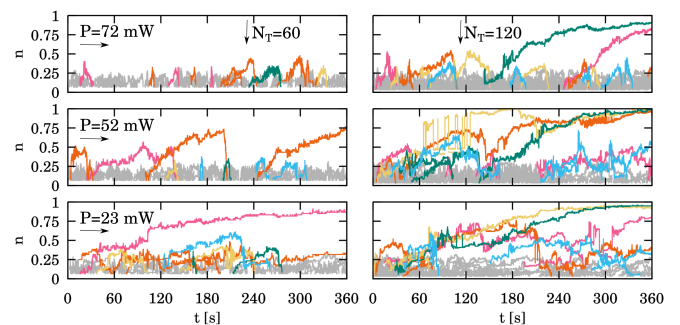


FIG. 2. Evolution of cluster size rescaled by the total number of agents in the arena ( $n=N/N_T$ ), for different activities ( $P$ ) in 6-minute-long experiments. The signal of clusters reaching a maximum size of at least a third of the total population is colored, while smaller clusters are represented in gray. The activity levels correspond to the highest, middle, and lowest illumination levels used in our experiments.

clusters exhibit gradual growth, eventually encompassing a significant portion of the particles in the system (see SM Video 1). Furthermore, some of these large clusters persist during the whole experimental realization, fluctuating in size as smaller clusters attach or detach from them (see SM video 2). In fact, the results of Fig. 2 suggest the existence of a transition from unstable to stable clustering as activity decreases and the population grows.

In the following, we investigate this transition by looking at the statistics of the clusters; in particular, we analyze the cluster duration  $t_d$  [47]. Fig. 3 (a-b) illustrates the survival function ( $P(t_d \geq t)$ , also called the complementary cumulative distribution function) of the cluster duration, namely the probability of finding a cluster that lasts longer than a given time ( $t$ ). Panel (a) presents the distributions for  $N_T=80$  and different intensities, while panel (b) focuses on an intermediate intensity level and

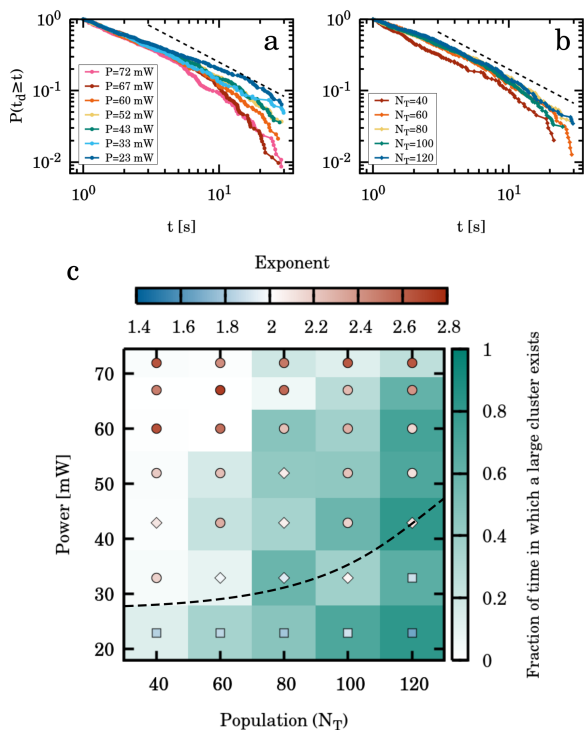


FIG. 3. (a): Cluster duration survival functions,  $P(t_d \geq t)$ , for  $N_T=80$  particles and different illumination intensities, and (b) for different number of particles at a given intensity ( $P=52$  mW). The dashed line represents a power law with exponent 1, which means an  $\alpha=2$  exponent for the PDF. (c): Phase diagram of the cluster stability. Circles represent  $\alpha > 2$  (i.e. unstable clusters), squares  $\alpha < 2$  (i.e. stable clusters), and diamonds are used for the transition region (i.e.  $\alpha = 2 \pm 0.1$ ). The color of the symbol indicates the exact value of  $\alpha$  as shown in the top colorbar. On the other side, the greenish color of each internal cell indicates the fraction of time in which we have at least one cluster larger than 33% of the total population. The dashed black line is a guide for the eye separating the two phases: stable clustering (low  $P$ , high  $N_T$ ) and unstable clustering (high  $P$ , low  $N_T$ ).

different populations. We observe a behavior compatible with a power-law distribution:  $\text{PDF}(t_d) \propto t_d^{-\alpha}$ . In case of the survival function  $P(t_d \geq t) = \int_t^\infty dt' \text{PDF}(t') \propto t^{-(\alpha-1)}$  so the exponent is reduced by 1. Importantly, we observe that  $\alpha > 2$  for scenarios with high activity and small population sizes and  $\alpha \leq 2$  for low activities and large population sizes. The latter corresponds to average cluster durations that diverge and correlates with the finding of stable clusters that do not disappear during the experiments. Fig. 3 (c) shows a sketch of the phase diagram based on the fitted exponents. Clearly, low light intensities and large population sizes lead to a region of stable clusters (bottom-right in the figure) whereas high light intensities and small population sizes (top-left), lead to unstable clusters. To establish another measure of the stability of clusters, we calculated the fraction of the time in which at least one cluster (larger than 33% of the total population) exists. The obtained results are also shown in Fig. 3 (c) corroborating the observation made using the exponents of the distribution.

*Kinetic model.*— Inspired by Refs. [48, 49], we propose a simple kinetic model aiming to capture the formation, growth, and destruction of a cluster within a ‘gas’ of free-moving particles. The idea is that the evolution of the cluster size  $N$  is governed by a balance between adsorption and desorption processes. First, we assume that each collision between a particle and a cluster results in particle entrapment. Therefore, the adsorption rate is approached by  $k_a = v \rho_g L$ , where  $L$  is the typical length of the cluster,  $v$  is the velocity of a free particle, and  $\rho_g$  represents the density of particles in the gas phase. Then, if the cluster area is  $A_c = L^2$ , and also  $A_c = N A_p / \Phi_c$ , where  $A_p$  is the area of a single particle, and  $\Phi_c$  is the packing fraction inside the cluster, it results that  $k_a = v \left( \frac{N_T - N}{A_T} \right) \sqrt{\frac{N A_p}{\Phi_c}}$ . In contrast, a particle trapped in a cluster experiences a fast diffusive process induced by the frequent collisions with its neighbors. To estimate the characteristic time of the desorption process, we assume that only surface particles depart from the cluster with a characteristic time  $\tau_d = A_{\text{acc}} / D$ , where  $A_{\text{acc}} = A_p / \Phi_c$  is the accessible area for a surface particle and  $D$  the diffusion coefficient of the hexbugs within the clusters. Thus, the zero-order desorption rate is  $k_d = \frac{D \Phi_c}{A_p}$ . Summing up, the cluster size  $N$  follows a simple kinetic adsorption-desorption equation:

$$\frac{dN}{dt} = v \frac{(N_T - N)}{A_T} \sqrt{\frac{N A_p}{\Phi_c}} - \frac{D \Phi_c}{A_p}, \quad (1)$$

After the arrangement of Eq.(1), we obtain that the kinetic evolution of  $n = N/N_T$  (the rescaled number of particles in a cluster) follows

$$\frac{dn}{d\tau} = (1 - n)n^{1/2} - \kappa, \quad (2)$$

with

$$\kappa = \frac{\Phi_c^{3/2} A_T}{A_p^{3/2}} \cdot \frac{1}{N_T^{3/2}} \cdot \frac{D}{v}, \quad (3)$$

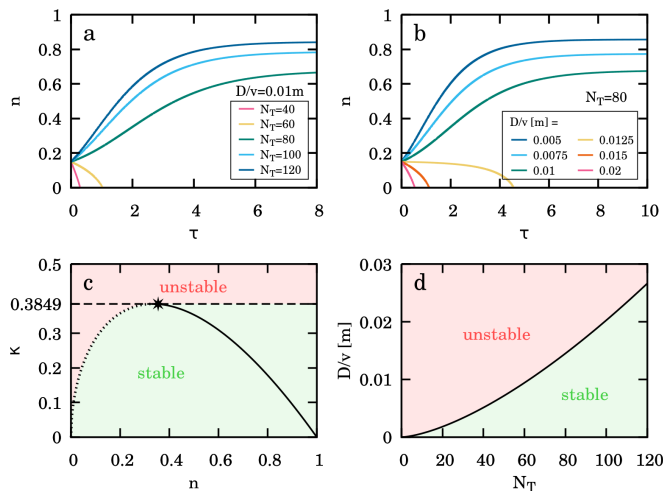


FIG. 4. Model prediction of the cluster size. In (a) results corresponding to the temporal evolution of the proportion of bugs in the cluster  $n=N/N_T$  for a fixed activity level  $D/v=0.01$  m and different  $N_T$ . In (b) similar plot for  $N_T=80$  and different values of  $D/v$ . Panel (c) illustrates a phase diagram in terms of  $\kappa$  and  $n$ . The green regions correspond to stable clustering, whereas the red ones correspond to cluster dissolution. The dashed line indicates the critical value  $\kappa_{\text{crit}}=0.3849$  above which clusters are always unstable. The dotted and continuous lines correspond  $\kappa=(1-n)n^{1/2}$ . The dotted line is the minimal cluster size necessary to observe clustering, and the continuous line represents the final cluster size as  $\tau \rightarrow \infty$ . The star indicates the crossover between these two trends. Panel (d) displays the same phase diagram but in terms of  $N_T$  and  $D/v$ .

and  $\tau=c_a t$  (for details see the SM). Thus, the kinetic control parameter  $\kappa$  mainly depends on three terms; the first one is a group of constants depending on the geometry of the bugs, size of the arena, etc.; the second depends on the population size ( $N_T$ ); and the third on  $D/v$ , which in turn, is related to the activity of the bugs, i.e. the light intensity.

Fig. S2 (a-b) examines the analytic solution of the kinetic model of Eq.(2). First, in Fig. S2 (a) we display the evolution of the cluster size  $n(\tau)$  keeping  $D/v=0.01$  m and varying  $N_T$ . As in the experimental case, when  $N_T$  increases, there is a transition from cluster dissolution ( $n(\tau) \rightarrow 0$ ) to cluster growth and stabilization. Similarly, in Fig. S2 (b) we observe the transition when keeping  $N_T=80$  and reducing  $D/v$ . The fact that clusters develop for low values of  $D/v$  suggests that the illumination intensity in the experiments positively correlates with  $D/v$ . This seems reasonable given the small dependence of  $v$  on the illumination intensity explained earlier (from 8 to 14 cm/s).

Examining Eq.(2) with more detail, we observe that the growth and formation of stable clusters depend on the specific value of the control parameter  $\kappa$  and the number of bugs in the initial cluster (Fig. S2 (c)). The plot shows a clear bifurcation at  $\kappa_{\text{crit}}=0.3849$ ; for higher val-

ues, clusters always disassociate, while for lower values they can be stable. To this end, it is necessary that the initial cluster size  $n_0$  is larger than the value given by  $\kappa=(1-n_0)n_0^{1/2}$  (dotted line in Fig. S2 (c)) or  $n_0=0.33$ . The final stable cluster size (indicated by the continuous line) is the solution of  $\kappa=(1-n)n^{1/2}$  that is higher than  $n=0.33$ .

In order to understand the behavior of the system depending on  $D/v$  and the population size  $N_T$ , we substitute the values of  $\kappa=0.3849$ ,  $\Phi_c$ ,  $A_T$ , and  $A_p$  to Eq. 3, obtaining the phase diagram of Fig. S2 (d). Analogously to the experiments, for small  $N_T$  and high values of  $D/v$  clusters disassociate, while for large  $N_T$  and low values of  $D/v$ , the formation of stable clusters is possible. Interestingly, taking  $N_T=80$  and  $v=10$  cm/s as an example, we obtain  $D \approx 14.5$  cm<sup>2</sup>/s, a figure that seems rather reasonable.

Aiming for a further test of the goodness of the model and taking advantage of the versatility of our experiment, we implement a specific analysis of the cluster dissolution dynamics using a population size of  $N_T=100$  bugs. We first apply maximum and minimum intensities to the two halves of the arena, hence facilitating cluster formation at the low-activity region (Fig. 5 (a-b)). When a single relatively large cluster forms (b), we switch to the highest light intensity in the whole arena (c) and we analyze the cluster dynamics for 6 minutes. We repeat this protocol 50 times obtaining the probability of disassociation (after 6 minutes) as a function of the initial cluster size

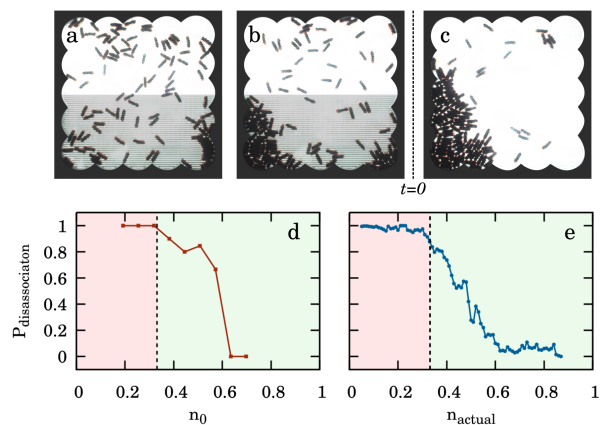


FIG. 5. Experiments implemented to test the cluster disassociation dynamics predicted by the model. We start with a homogeneously distributed sample of  $N_T=100$  and we apply the highest intensity of light to one half of the arena, and the lowest to the other. After less than one minute a cluster develops in the darker half (b). Then ( $t=0$ ), we switch to homogeneous illumination with the highest intensity and analyze the cluster dynamics (c). In (d) and (e) we represent, respectively, the probability of disassociation as a function of the initial cluster size and as a function of the cluster size at each timestep (sampled every 0.033 s). The dashed lines show the prediction of the kinetic model for the critical cluster size above which clusters are stable.

( $n_0$ ) as shown in panel (d). Importantly, the value of  $n_0$  at which the probability starts to decay nicely resembles the value offered by the model (0.33) if we consider the highest value of  $D/v$  that allows the development of stable clusters. An alternative method to estimate the disassociation probability would imply considering all the cluster sizes after the switch to the highest light intensity as initial sizes and then determining the probability of dissolution with much more data. Clearly, the results of this method (Fig. 5 (e)) resemble the previous one, confirming the predictive character of our model.

In summary, in this work, we use a new type of active particles (photoactive and macroscopic) to thoroughly analyze cluster dynamics. We identify the existence of a phase (for low particle activities and large population sizes) in which clusters are stable. On the contrary, for high particle activities and low population sizes, clusters dissolve. This behavior is reproduced by means of a sim-

ple kinetic model that includes absorption and desorption rates of individual particles. The model reveals an undiscovered dependence of the cluster stability on the initial cluster size that is posteriorly corroborated by new experiments in which we take advantage of the external control of the particle's activity.

We especially acknowledge Luis Fernando Urrea for technical help and Lucia Sastre for helping in the preparation of the particles. This project has received funding from the European Union's Horizon 2020 research and innovation programme under the Marie Skłodowska-Curie grant agreement No. 101067363 named PhotoActive and the Spanish Government, through grant No. PID2023-146422NB-I00 supported by MICIU/AEI/10.13039/501100011033. A. K. acknowledges the Asociación de Amigos, Universidad de Navarra, for his grant.

- 
- [1] S. Palagi *et al.*, Structured light enables biomimetic swimming and versatile locomotion of photoresponsive soft microrobots, *Nat. Mater.* **15**, 647 (2016).
- [2] W. Hu, G. Z. Lum, M. Mastrangeli, and M. Sitti, Small-scale soft-bodied robot with multimodal locomotion, *Nature* **554**, 81 (2018).
- [3] T. Xu, J. Zhang, M. Salehizadeh, O. Onaizah, and E. Diller, Millimeter-scale flexible robots with programmable three-dimensional magnetization and motions, *Sci. Robot.* **4**, eaav4494 (2019).
- [4] J. Cui, T.-Y. Huang, Z. Luo, P. Testa, H. Gu, X.-Z. Chen, B. J. Nelson, and L. J. Heyderman, Nanomagnetic encoding of shape-morphing micromachines, *Nature* **575**, 164 (2019).
- [5] M. Z. Miskin, A. J. Cortese, K. Dorsey, E. P. Esposito, M. F. Reynolds, Q. Liu, M. Cao, D. A. Muller, P. L. McEuen, and I. Cohen, Electronically integrated, mass-manufactured, microscopic robots, *Nature* **584**, 557 (2020).
- [6] H. H. Wensink and H. Löwen, Aggregation of self-propelled colloidal rods near confining walls, *Phys. Rev. E* **78**, 031409 (2008).
- [7] I. Buttinoni, J. Bialké, F. Kümmel, H. Löwen, C. Bechinger, and T. Speck, Dynamical clustering and phase separation in suspensions of self-propelled colloidal particles, *Phys. Rev. Lett.* **110**, 238301 (2013).
- [8] J. Palacci, S. Sacanna, A. P. Steinberg, D. J. Pine, and P. M. Chaikin, Living crystals of light-activated colloidal surfers, *Science* **339**, 936 (2013).
- [9] C. Lozano, B. Ten Hagen, H. Löwen, and C. Bechinger, Phototaxis of synthetic microswimmers in optical landscapes, *Nat. Commun.* **7**, 12828 (2016).
- [10] H. R. Vutukuri, M. Lisicki, E. Lauga, and J. Vermant, Light-switchable propulsion of active particles with reversible interactions, *Nat. Commun.* **11**, 2628 (2020).
- [11] J. Arlt, V. A. Martinez, A. Dawson, T. Pilizota, and W. C. K. Poon, Painting with light-powered bacteria, *Nat. Commun.* **9**, 768 (2018).
- [12] A. Be'er and G. Ariel, A statistical physics view of swarming bacteria, *Mov. Ecol.* **7**, 1 (2019).
- [13] Y. Martínez-Ratón and E. Velasco, Enhanced stability of the tetratic phase due to clustering, *Phys. Rev. E* **79**, 011711 (2009).
- [14] C. Scholz, M. Engel, and T. Pöschel, Rotating robots move collectively and self-organize, *Nat. Commun.* **9**, 931 (2018).
- [15] M. Bär, R. Großmann, S. Heidenreich, and F. Peruani, Self-propelled rods: Insights and perspectives for active matter, *Annu. Rev. Condens. Matter Phys.* **11**, 441 (2020).
- [16] H. Soni, N. Kumar, J. Nambisan, R. K. Gupta, A. K. Sood, and S. Ramaswamy, Phases and excitations of active rod-bead mixtures: simulations and experiments, *Soft Matter* **16**, 7210 (2020).
- [17] M. Mohammadi, K. Harth, D. Puzyrev, T. Hanselka, T. Trittel, and R. Stannarius, Dynamics of self-propelled particles passing a bottleneck, *New J. Phys.* **22**, 123025 (2020).
- [18] H. Oh, A. R. Shirazi, C. Sun, and Y. Jin, Bio-inspired self-organising multi-robot pattern formation: A review, *Rob. Auton. Syst.* **91**, 83 (2017).
- [19] G. Ariel and A. Ayali, Locust collective motion and its modeling, *PLoS Comput. Biol.* **11**, e1004522 (2015).
- [20] F. Ginelli, F. Peruani, M.-H. Pillot, H. Chaté, G. Theraulaz, and R. Bon, Intermittent collective dynamics emerge from conflicting imperatives in sheep herds, *PNAS* **112**, 12729 (2015).
- [21] B. Liebchen and H. Löwen, Synthetic chemotaxis and collective behavior in active matter, *Acc. Chem. Res.* **51**, 2982 (2018).
- [22] I. Mori and Y. Ohshima, Neural regulation of thermotaxis in *Caenorhabditis elegans*, *Nature* **376**, 344 (1995).
- [23] B. Liebchen, P. Monderkamp, B. Ten Hagen, and H. Löwen, Viscotaxis: Microswimmer navigation in viscosity gradients, *Phys. Rev. Lett.* **120**, 208002 (2018).
- [24] M. Sun, X. Fan, X. Meng, J. Song, W. Chen, L. Sun, and H. Xie, Magnetic biohybrid micromotors with high maneuverability for efficient drug loading and targeted drug delivery, *Nanoscale* **11**, 18382 (2019).
- [25] F. Siebers, A. Jayaram, P. Blümler, and T. Speck,

- Exploiting compositional disorder in collectives of light-driven circle walkers, *Sci. Adv.* **9**, eadf5443 (2023), <https://www.science.org/doi/pdf/10.1126/sciadv.adf5443>.
- [26] M. Mijalkov, A. McDaniel, J. Wehr, and G. Volpe, Engineering sensorial delay to control phototaxis and emergent collective behaviors, *Phys. Rev. X* **6**, 011008 (2016).
- [27] M. Leyman, F. Ogemark, J. Wehr, and G. Volpe, Phototactic robot tunable by sensorial delays, arXiv preprint arXiv:1807.11765 (2018).
- [28] M. Rey, G. Volpe, and G. Volpe, Light, matter, action: Shining light on active matter, *ACS Photonics* **10**, 1188 (2023).
- [29] <https://www.hexbug.com/nano.html>.
- [30] G. A. Patterson, P. I. Fierens, F. Sangiuliano Jimka, P. G. König, A. Garcimartín, I. Zuriguel, L. A. Pugnaloni, and D. R. Parisi, Clogging transition of vibration-driven vehicles passing through constrictions, *Phys. Rev. Lett.* **119**, 248301 (2017).
- [31] A. Deblais, T. Barois, T. Guerin, P. H. Delville, R. Vaudaine, J. S. Lintuvuori, J. F. Boudet, J. C. Baret, and H. Kellay, Boundaries control collective dynamics of inertial self-propelled robots, *Phys. Rev. Lett.* **120**, 188002 (2018).
- [32] T. Barois, J. F. Boudet, N. Lanchon, J. S. Lintuvuori, and H. Kellay, Characterization and control of a bottleneck-induced traffic-jam transition for self-propelled particles in a track, *Phys. Rev. E* **99**, 052605 (2019).
- [33] T. Barois, J. F. Boudet, J. S. Lintuvuori, and H. Kellay, Sorting and extraction of self-propelled chiral particles by polarized wall currents, *Phys. Rev. Lett.* **125**, 238003 (2020).
- [34] M. Leoni, M. Paoluzzi, S. Eldeen, A. Estrada, L. Nguyen, M. Alexandrescu, K. Sherb, and W. W. Ahmed, Surfing and crawling macroscopic active particles under strong confinement: Inertial dynamics, *Phys. Rev. Res.* **2**, 043299 (2020).
- [35] J. F. Boudet *et al.*, From collections of independent, mindless robots to flexible, mobile, and directional superstructures, *Sci. Robot.* **6**, eabd0272 (2021), <https://www.science.org/doi/pdf/10.1126/scirobotics.abd0272>.
- [36] P. Baconnier, D. Shohat, C. H. López, C. Coulais, V. Démery, G. Düring, and O. Dauchot, Selective and collective actuation in active solids, *Nat. Phys.* **18**, 1234 (2022).
- [37] G. A. Patterson and D. R. Parisi, Fundamental diagram of vibration-driven vehicles, arXiv preprint arXiv:2311.01211 (2023).
- [38] A. Altshuler, O. L. Bonomo, N. Gorohovsky, S. Marchini, E. Rosen, O. Tal-Friedman, S. Reuveni, and Y. Roichman, Environmental memory facilitates search with home returns, *Phys. Rev. Res.* **6**, 023255 (2024).
- [39] Y. Xi, T. J. Jones, R. Huang, T. Marzin, and P.-T. Brun, Emergent intelligence of buckling-driven elasto-active structures - preprint, <https://arxiv.org/abs/2404.10614>.
- [40] N. A. M. Araújo *et al.*, Steering self-organisation through confinement, *Soft Matter* **19**, 1695 (2023).
- [41] R. C. Maloney, G.-J. Liao, S. H. L. Klapp, and C. K. Hall, Clustering and phase separation in mixtures of dipolar and active particles, *Soft Matter* **16**, 3779 (2020).
- [42] S. Thapa, B.-E. Pinchasik, and Y. Shokef, Emergent clustering due to quorum sensing interactions in active matter, *New J. Phys.* **26**, 023010 (2024).
- [43] M. Becton, J. Hou, Y. Zhao, and X. Wang, Dynamic clustering and scaling behavior of active particles under confinement, *Nanomaterials* **14**, 144 (2024).
- [44] L. Caprini, D. Breoni, A. Ldov, C. Scholz, and H. Löwen, Dynamical clustering and wetting phenomena in inertial active matter, *Commun. Phys.* **7**, 343 (2024).
- [45] See Supplemental Material at XXX for experimental videos and details on the experimental setup and particle characterization. The influence of the wall structure is also discussed there. Furthermore, we give a detailed description of the kinetic model.
- [46] N. Kumar, H. Soni, S. Ramaswamy, and A. K. Sood, Flocking at a distance in active granular matter, *Nat. Commun.* **5**, 4688 (2014).
- [47] The first 2 minutes of the 6-minute-long experiments were removed from the analysis in order to prevent the inclusion of a transient that would depend on the initial sample preparation.
- [48] F. Peruani, L. Schimansky-Geier, and M. Baer, Cluster dynamics and cluster size distributions in systems of self-propelled particles, *Eur. Phys. J. Special Topics* **191**, 173 (2010).
- [49] F. Ginot, I. Theurkauff, F. Detcheverry, C. Ybert, and C. Cottin-Bizonne, Aggregation-fragmentation and individual dynamics of active clusters, *Nat. Commun.* **9**, 696 (2018).

## Supplemental Material for “Cluster dynamics in macroscopic photoactive particles”

Sára Lévy,\* Axel Katona, Hartmut Löwen, Raúl Cruz Hidalgo, Iker Zuriguel

\*Electronic address: slevey@unav.es

### S I. EXPERIMENTAL SETUP

Fig. S1 (a) shows the side view of the experimental setup. The glass sheets and the illumination panel are mounted on an aluminum scaffold. The imaging system is placed beneath the experiment. The illumination panel can be easily lifted as shown in panel (b), and the upper glass sheet can be slid to manipulate the particles. Additionally, two fans are mounted on the top of the illumination panel to prevent overheating.

The illumination panel is made of LED lines, mounted on an aluminum plate, controlled by ESP32 microcontrollers. Serial port communication method was established between a computer using LabView and the microcontrollers. By this we can tune the illumination intensity of each line individually, using pulse-width modulation.

### S II. VIDEOS

#### SM Videos

**Video 1** shows an experiment conducted with 120 particles under low illumination intensity (23 mW). The particles were initially arranged in rows, evenly distributed between the two halves of the system, facing towards the center. Smaller clusters formed and destroyed throughout the experiment; then one cluster gradually grew and became stable, ultimately incorporating around 75% of the particles. The experimental photo shown in Fig. 1 (b) of the main manuscript was captured during this experiment (see at 1’28”).

**Video 2** shows an experiment with 100 particles under medium illumination intensity (43 mW). Throughout the experiment, clusters formed and destroyed, without any stable clustering observed. Towards the end of the video, we present a case, where two clusters are merged, resulting in the creation of a relatively large cluster that was later destroyed.

**Video 3** depicts an experiment with 60 particles under high illumination intensity (72 mW). The high particle activity leads to the rapid formation and destruction of small clusters. No cluster becomes stabilized within the experimental duration.

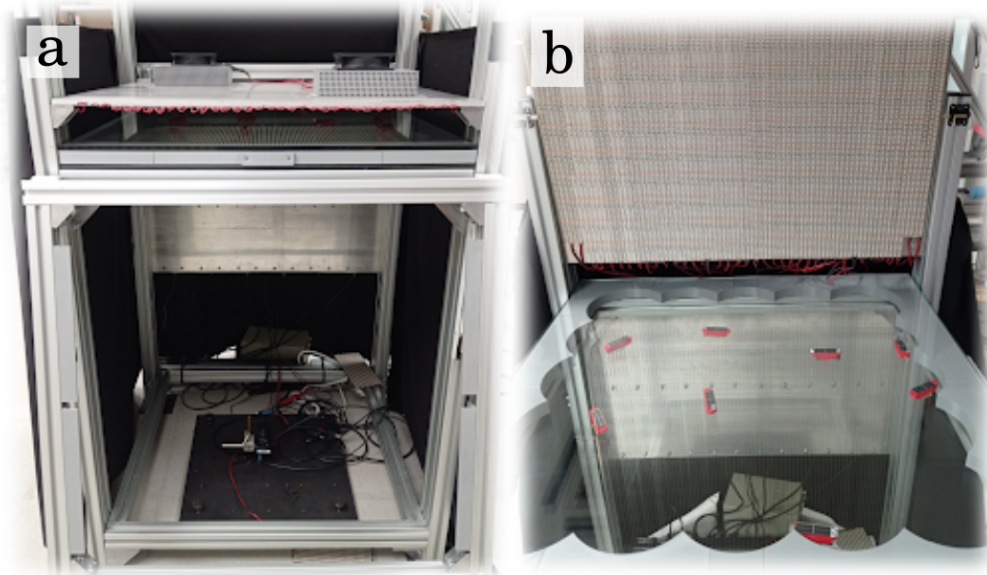


FIG. S1. Photos of the experimental setup. (a): Side view. (b): Top view with the illumination panel lifted, showing a few particles and the enclosing wall structure.

### S III. THE KINETIC MODEL

Aiming for a better understanding of the time evolution of clusters in the system, we have developed a simple kinetic model that describes the fundamental processes responsible for cluster growth and destruction. Note that this model is deterministic as it does not include noise or randomness of any nature. Obviously, this is not the case in real experiments but still, we believe it is useful to understand the observed behavior.

Basically, we propose that the variation of the number of particles in a cluster is governed by a balance of adsorption and desorption of active particles. Then, to estimate the rate of particles adsorbed by the cluster, we assume that every collision of a free particle with a cluster results in particle entrapment. The collision rate depends on the relative velocity of the cluster and the single particle, the particle density in the ‘gas’ phase ( $\rho_g$ ), and the typical length of the cluster ( $L$ ). The absorption rate is thus  $k_a = v\rho_g L$ . We assume that the relative velocity of the cluster and the single particle is mostly governed by the latter with velocity  $v$ . The particle concentration in the gas phase is  $\rho_g = (N_T - N)/A_T$ , where  $N_T$  is the total number of particles in the system,  $N$  is the number of particles in the cluster and  $A_T$  is the total area of the arena. Then, we relate the length of the cluster with the area of the cluster by assuming  $A_c = L^2$ . In addition, the area of the cluster can be expressed by  $A_c = NA_p/\Phi_c$ , where  $A_p$  is the area of a single particle and  $\Phi_c$  is the packing fraction within the cluster. From this  $L = \frac{N^{1/2}A_p^{1/2}}{\Phi_c^{1/2}}$  resulting in the absorption rate:

$$k_a = v \cdot \frac{N_T - N}{A_T} \cdot \frac{N^{1/2}A_p^{1/2}}{\Phi_c^{1/2}} = \frac{vA_p^{1/2}}{\Phi_c^{1/2}A_T}(N_T - N)N^{1/2}. \quad (\text{S1})$$

To estimate the rate of the departure of active particles from the cluster, we assume that the motion of the surface particles in the cluster can be described within the diffusion approximation. The rate of desorption of a particle from the cluster is  $k_d = D/A_{\text{acc}}$ , where  $D$  is the coefficient of diffusion of particles in the cluster surface, and  $A_{\text{acc}}$  is the accessible area for a cluster particle:  $A_{\text{acc}} = \frac{A_p}{\Phi_c}$ . This results in the desorption rate:

$$k_d = \frac{D\Phi_c}{A_p}. \quad (\text{S2})$$

The variation of the number of particles in a cluster is then:

$$\frac{dN}{dt} = k_a - k_d = \frac{vA_p^{1/2}}{\Phi_c^{1/2}A_T}(N_T - N)N^{1/2} - \frac{D\Phi_c}{A_p}. \quad (\text{S3})$$

Introducing  $n = N/N_T$ , as the relative cluster size, the equation takes the following form:

$$\frac{dn}{dt} = c_a(1 - n)n^{1/2} - c_d, \quad (\text{S4})$$

with  $c_a = \frac{vA_p^{1/2}N_T^{1/2}}{\Phi_c^{1/2}A_T}$  and  $c_d = \frac{D\Phi_c}{A_pN_T}$ , containing fixed parameters and the two variables we change in the experiments, namely the total number of particles ( $N_T$ ), and the illumination intensity. The model reflects the latter through  $D$  and  $v$ . Rescaling the time to  $\tau = c_a t$ , the equation turns into:

$$\frac{dn}{d\tau} = (1 - n)n^{1/2} - \kappa, \quad (\text{S5})$$

where

$$\kappa = c_d/c_a = \frac{\Phi_c^{3/2}A_T}{A_p^{3/2}} \cdot \frac{1}{N_T^{3/2}} \cdot \frac{D}{v}, \quad (\text{S6})$$

where the constants (first term) and the parameters changed in the experiments (second and third terms) are separated.

If  $\kappa > (1 - n)n^{1/2}$  (red area in Fig. S2 (a)), thus  $\frac{dn}{d\tau} < 0$ , clusters are not stable, they disassociate and disappear. Otherwise, when  $\kappa < (1 - n)n^{1/2}$ , hence  $\frac{dn}{d\tau} > 0$ , then clusters grow and stabilize (green area in Fig. S2 (a)). This means that for values of  $\kappa$  above the critical value  $\kappa_{\text{crit}} = 0.3849$ , clusters always decay, and for values of  $\kappa$  below the critical value, clusters grow and stabilize if they start from a size larger than an initial critical cluster size,  $n_{\text{crit}}$  (see



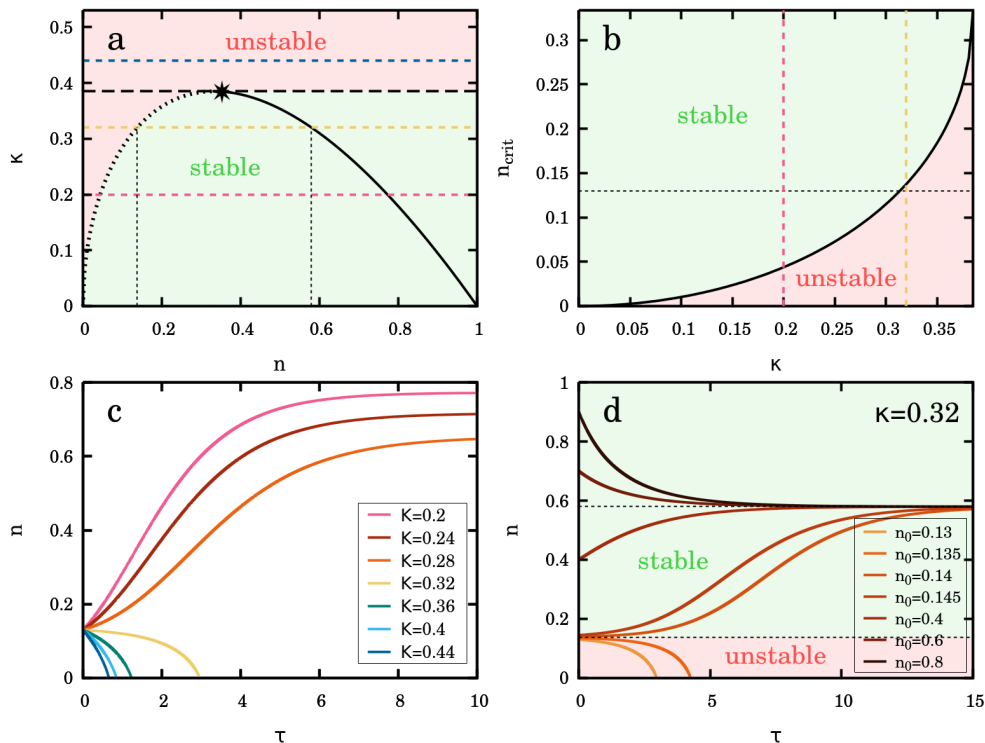


FIG. S2. (a): Phase diagram identical to the one presented in Fig. 4 (c) of the main paper but with the inclusion of several reference (dashed) lines for several values of  $\kappa$  that are analyzed in the other panels. (b): The critical initial cluster size,  $n_{\text{crit}}$  as a function of  $\kappa$ . Recall that  $\kappa_{\text{crit}}=0.3849$ , so  $n_{\text{crit}}$  diverges at this value. The yellow and pink dashed lines show the same value of  $\kappa$  as in panel (a). (c): Time evolution of clusters predicted by the model for different  $\kappa$  values, starting from an initial cluster size  $n_0=0.13$ . The pink, yellow, and dark blue curves correspond to the lines of the same color in panels (a-b). Note that in panel (b) there is no blue curve as it is beyond  $\kappa_{\text{crit}}$ . (d): Time evolution of clusters predicted by the model for  $\kappa=0.32$  (yellow line in panels (a-b)), starting from different initial cluster sizes ( $n_0$ ). Below  $n_{\text{crit}}=0.1377$  (light orange lines) stable clusters do not develop, while above that threshold stable clusters develop.

dotted curve in Fig. S2 (a)). This behavior is better understood by looking at Fig. S2 (b), where we only represent the minimum cluster size necessary to reach stable clustering as a function of  $\kappa$ . Clearly,  $n_{\text{crit}}$  diverges for  $\kappa_{\text{crit}} = 0.3849$ , as for values of  $\kappa$  above this threshold, clusters are not stable, no matter their size.

Note that the parameter  $\kappa$  decreases as we increase the population in the system and decrease the particle activity (thus decreasing  $D/v$ ). This means that the kinetic model captures the same transition between unstable and stable clustering that we have seen in the experiments. Then, aiming a better understanding of the model, in Fig. S2 (c) we show the time evolution of clusters for different values of  $\kappa$ , starting from an initial cluster size  $n_0 = 0.13$  (dashed line in panel (b)). This initial cluster size allows the formation of stable clusters for values of  $\kappa$  slightly below 0.32. For cases with higher values of  $\kappa$ , thus lower populations and higher particle activities, the formation of stable clusters is no longer possible, the desorption term is dominating in their time evolution.

To stress the importance of initial cluster size  $n_0$ , Fig. S2 (d) shows the time evolution of clusters for  $\kappa = 0.32$  (yellow line in panels (a) and (b)), starting from different initial sizes. One can see, that for  $n_0$  values below  $n_{\text{crit}}(\kappa=0.32) = 0.1377$  (light oranges), the clusters are not stable and disappear after a relatively short time. Above this critical initial cluster size (dark oranges) clusters grow and stay stable at the final stable cluster size (0.5797 for  $\kappa=0.32$ ). When the initial cluster size is larger than this value (dark reds), the model predicts an initial decrease in the cluster size, stabilized at this value.

#### S IV. INFLUENCE OF THE WALL STRUCTURE ON THE CLUSTERING DYNAMICS

As it is broadly known, self-propelled particles tend to cluster at the walls of the arena as, when they collide perpendicularly, they need several seconds to change the direction of motion. This is typically the seed for the cluster generation which occurs when other particles interact with this one. An alternative scenario that may lead to the

creation of a cluster is when two particles moving along the wall in opposite directions, collide and start pushing each other. As a result of this, the confining walls have significant importance in the observed development and growth of clusters. Indeed, when the arena is circular, clustering is extremely favored, occurring for almost all activities and densities. One would observe the same behavior in the case of straight walls, with particles accumulating at the corners. In order to prevent this, and redirect the particles to the center of the arena, flower-shaped geometries were ideated.

In our experiments, the wall structure is made of small, curved segments (with a diameter of 17 cm, which is around 3 times the length of particles). All the experiments we present in the paper were done with the structure visible in Fig. S3 (a,c) in which each side of the arena contains 5 of these curved segments. To test the generality of the observed behavior we experimented with two other structures. In one case (Fig. S3 (b)) we increased the separation between the circular segments (maintaining the curvature), hence reducing the number of them that fit in each lateral side (from 5 to 4). In the other case, we kept the original structure (curvature and separation of segments) but reduced the arena size by approximately 40% as can be seen in panel (d).

In Fig. S3 (a-d) we show the cluster duration survival functions for the three different wall structures. In both cases, we repeated 5 experiments for each illumination level. In the case of the (b) structure, we have experimented with 80 particles, while for the (d) structure we experimented with 100 bugs. To facilitate the comparison, in panels (a,c) we present the results of these two populations for the original wall structure. Comparing panels (a,b) we observe that the arena with 4 curved segments leads to slightly longer (more stable) clusters than the arena with 5 curved segments. This can be understood if we think that in the 4-segment arena, the area covered for each one of these circles is larger than in the 5-segment arena, a feature that could probably favor the stability of the clusters formed inside them. Similarly, reducing the arena surface but keeping the same boundary shape (panels c,d) seems to slightly increase the cluster stability; a behavior that correlates with the increment of the density of particles within the arena which, by the way, is a feature covered by the model.

In any case, the behavior encountered for these other two wall geometries is similar to that reproduced in the main manuscript, evidencing a transition from cluster dissolution to cluster stabilization as it decreases the intensity of light.

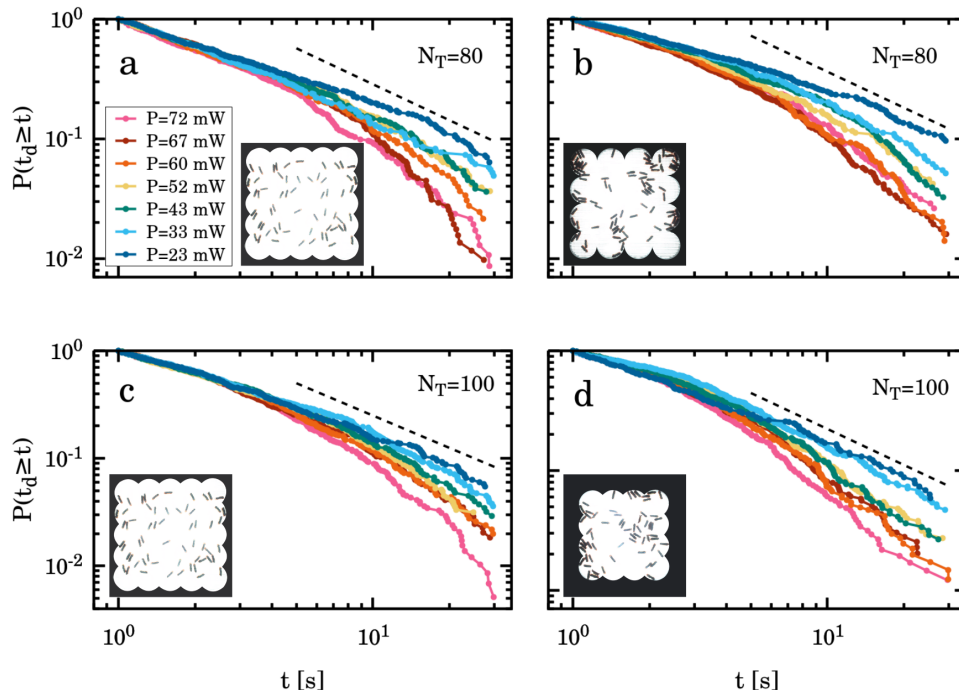


FIG. S3. Survival function of the cluster duration for different wall structures. In panels (a) and (b) we work with  $N_T = 80$  and compare arenas in which we increase the separation between the curved segments. In panels (c) and (d) we work with  $N_T = 100$  and we compare arenas with different surfaces while keeping the wall geometry. Different light intensities are implemented as indicated in the legend of panel (a).

## S V. CHARACTERIZATION OF THE MOTION OF INDIVIDUAL PARTICLES

Before studying the collective behavior of the photosensitive bugs, we characterize their individual motion and obtain information about their velocity and preferred directionality. Importantly, by adding the plastic cap and the photovoltaic cell to the Hexbugs, we alter their mass distribution, which, in most cases, makes them rotate. We try to eliminate this by adding a counterbalance and small additional masses to the particles. We calibrate the position of the small masses such that the bug would be able to maintain a relatively straight trajectory under the highest level of illumination ( $P=72$  mW), although in some cases particles show a tendency of rotation.

In order to quantify the velocity and the persistence of the directionality of the bugs, we performed several experiments with all of the particles. In groups of 8, the particles moved within the arena under three different homogeneous illumination intensities for two minutes. We repeated this protocol 4 times for all groups. Then, we detect the trajectories (see Fig. S4 (a)) and, after identifying all collisions (particle-particle and particle-wall), we obtain the segments of the trajectories between collisions (panel (b)). For all the segments we calculate the velocity and the directionality (based on the change in velocity direction) of the particles, as presented in panels (c-d). Therefore, in the plots of Fig. S4(c-d), the results presented for each illumination intensity were taken from 8 experimental minutes in total.

The particle which behavior is represented in Fig. S4 displays a motion that is considered as straight. Indeed, segments persistently have an angular velocity smaller than 0.5 rad/s. However, this is not always the case and each agent can behave in very different manner. In Fig. S5, we show the angular velocities of other particles to exemplify the different types of behavior encountered among our bugs. In panels (a-b) we show particles that consistently tend to rotate clockwise or counterclockwise as evidenced by the absolute value of the angular velocity which is persistently larger than 0.5 rad/s. Importantly, in these particles the directionality does not change with the activity level. However, there are other particles whose rotation direction changes as with the illumination intensity (panels (c-d)).

Based on these encountered behavior, we grouped our 200 particles into different subsets: around 50% of the particles move more or less straightly (Fig. S4), 22% tend to rotate counterclockwise (Fig. S5 (a)), another 22% clockwise (Fig. S5 (b)), and around 6% of the particles change the direction of rotation as we change the illumination intensity (Fig. S5 (c-d)). In terms of the magnitude of the velocities, we have only seen a slight variation among different particles used, clearly showing increasing speeds with increasing illumination intensity.

In the experiments presented in the manuscript, for cases with  $N_T \leq 60$ , we used particles exclusively from the first

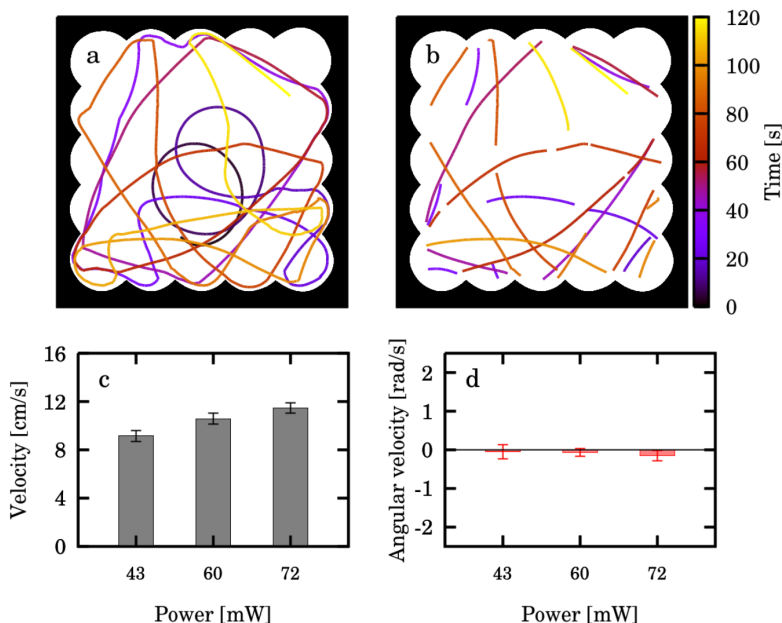


FIG. S4. Characterization of a single particle. (a): Trajectory under homogeneous illumination ( $P=72$  mW) for a 2-minute experiment. Colors represent the time. (b): Segments of the same trajectory. Particle-wall and particle-particle collisions were removed. (c): Average velocity of the same particle calculated for all the non-collisional segments of 4 repetitions of 2-minute-long experiments. (d): Average angular velocity for the same particle. As the values obtained are small and persistent over different realizations, this particle is considered to move along relatively straight lines.

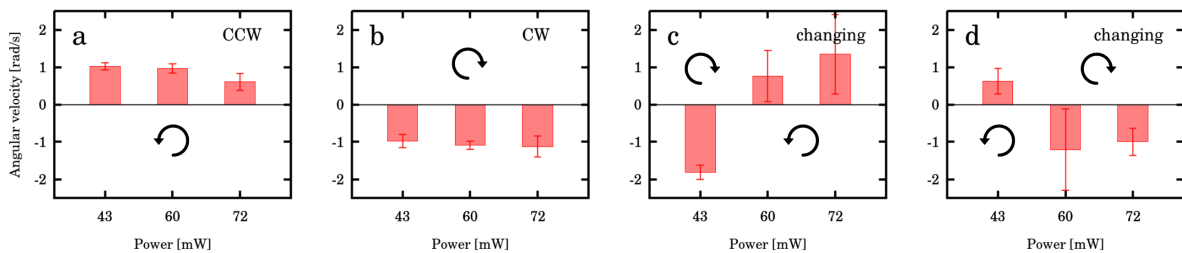


FIG. S5. Angular velocities of different particles obtained by repeating 2-minute-long experiments 4 times for three different homogeneous illumination intensities. (a): As the values are positive and relatively large (larger than 0.5 rad/s), this particle is considered to show a tendency to counterclockwise rotation. (b): Bug with a tendency to rotate clockwise. (c-d): Examples of particles with a changing rotational tendency. As we increase the illumination intensity, the direction of the rotation changes from CW to CCW or vice versa.

group (straight motion), while for higher populations we took particles from both of the groups. In terms of the collective behavior and the cluster dynamics, we have not seen any important differences that could be related to the specific composition of the population. However, as particles collide frequently, small alterations of the mass distribution may happen, causing some particles (usually less than 10% of the population) to develop strong rotation (as can be seen in some of the videos). These particles were replaced by new ones during the experiments.

## S VI. CLUSTER DETECTION METHOD

In order to study the cluster dynamics the particles were not tracked individually. Instead, patches of particles in contact with one another were detected with conventional image detection methods, due to the relatively high contrast between particle-occupied and empty regions. The number of particles constituting a patch is estimated from its area. For each frame of the recorded videos, we identify these patches and for further analysis, we consider only those that contain at least 4 particles. We then create a virtual network in which the nodes are the detected patches. Two nodes are connected by a link if they are from subsequent frames and have at least 30% overlap (this means that, the areas of the patches in consecutive frames overlap at least 30%). In this way linked parts of the network will represent the time evolution of a given patch. We apply a clustering algorithm to find the connected components in the network, with the criteria that a cluster should be at least 1 second long. If a connected component has branches longer than 2 seconds, we treated the branch as an individual cluster. By applying this method, properties such as duration, size, and the temporal evolution of all clusters can be quantified.